



Search for WH associated production with 5.3 fb^{-1} of Tevatron data

(Dated: July 21, 2010)

We present a search for WH production in $p\bar{p}$ collisions at a center of mass energy of $\sqrt{s} = 1.96 \text{ TeV}$ in data recorded by the DØ experiment corresponding to an integrated luminosity of 5.3 fb^{-1} . Multivariate techniques are applied to events containing one lepton, an imbalance in transverse energy and one or two tagged b -jets to discriminate the potential WH signal from standard-model backgrounds. Good agreement is observed between data and the expected background, and we set a combined observed (expected) upper limit of 4.1 (4.8) for $m_H = 115 \text{ GeV}$ at 95% C.L. on the ratio of $\sigma(p\bar{p} \rightarrow WH) \times \mathcal{B}(H \rightarrow b\bar{b})$ to its standard-model prediction.

Preliminary Results for the ICHEP 2010 Conference

The only unobserved particle of the standard model (SM) is the Higgs boson, which originates from the spontaneous breaking of electroweak symmetry. Its observation would confirm the hypothesis that the Higgs mechanism generates the masses of the weak gauge bosons, and also provides an explanation for the finite masses of fermions via their Yukawa couplings to the Higgs boson. The mass of the Higgs boson (m_H) is not predicted in the SM, but the combination of results from direct searches at the CERN e^+e^- Collider (LEP) [1] and precision measurements of other electroweak parameters constrain m_H to $114.4 < m_H < 186$ GeV at 95% C.L. [2]. While the region (162–166 GeV) is excluded at 95% C.L. by the CDF-D0 combined analysis [3], the remaining allowed mass range is being probed further at the Fermilab Tevatron Collider. The associated production of a Higgs boson and a W boson is among the cleaner Higgs channels at the Tevatron, and has the largest yield for the product of the cross section and branching fraction of $H \rightarrow b\bar{b}$ for $m_H < 125$ GeV. Several searches for WH production have already been published at a $p\bar{p}$ center-of-mass energy of $\sqrt{s} = 1.96$ TeV. Three of these [4–6] use subsamples (0.17 fb^{-1} , 0.44 fb^{-1} , and 1.1 fb^{-1}) of the data analyzed in this paper, while three others from the CDF collaboration are based on 0.32 fb^{-1} , 0.95 fb^{-1} and 2.7 fb^{-1} of integrated luminosity [7–9].

We present a new search using a multivariate approach in 5.3 fb^{-1} of data. The search is based on events with one charged lepton (ℓ , being e or μ), an imbalance in transverse energy (\cancel{E}_T) that arises from the neutrino in the $W \rightarrow \ell\nu$ decay, and either two or three jets, with one or two of these jets selected as a candidate b -quark jet (b -tagged).

The channels are separated into orthogonal selections of events with exactly one b -tagged jet and with two b -tagged jets. In events with two b -tagged jets, the dominant backgrounds are from $Wb\bar{b}$, $t\bar{t}$ and single top-quark production. In single b -tagged events there are two important sources of backgrounds. The first is multijet events, where a semileptonic hadron decay or parton-jet is misidentified as an isolated lepton. Second is W production in association with c -quark or light-quark jets. We use a random forest (RF) multivariate technique [10, 11] to separate the SM background from signal in the selected events and search for an excess, expected primarily at large values of the RF discriminant. A separate RF discriminant is created for each combination of final state jet multiplicity (2 or 3), lepton flavor (e or μ), and number of b -tagged jets (1 or 2). Two-jet events are further subdivided into data-taking epochs when creating RF discriminants, for a total of 12 independent channels. All channels are considered simultaneously when performing our search and final limit setting.

The analysis relies on the following components of the D0 detector [12]: a central-tracking system, which consists of a silicon microstrip tracker (SMT) and a central fiber tracker (CFT), both located within a 2 T superconducting solenoidal magnet; a liquid-argon/uranium calorimeter consisting of a central section (CC), covering pseudorapidity $|\eta| < 1.1$ relative to the center of the detector [13], and two end calorimeters (EC) extending coverage to $|\eta| < 4.0$, all housed in separate cryostats [14], with scintillators between the CC and EC cryostats providing sampling of developing showers at $1.1 < |\eta| < 1.4$; a muon system located beyond the calorimetry, and consists of layers of tracking detectors and scintillation trigger counters before and after the 1.8 T iron toroids.

The luminosity is measured using plastic scintillator arrays located in front of the EC cryostats at $2.7 < |\eta| < 4.4$. We reject data in which the tracking (CFT and SMT), calorimeter or muon information may have been compromised. The trigger and data acquisition systems are designed to accommodate the high instantaneous luminosities of Run II.

Events in the electron channel are triggered by a logical OR of several triggers requiring an electromagnetic (EM) object and one jet. Trigger efficiencies are taken into account in the simulation through a reweighting of events, based on an efficiency derived from data, and parametrized as a function of electron η , azimuth ϕ , and jet p_T .

We accept muon channel events from any trigger, and expect this combination of all triggers to be fully efficient with respect to our event selection criteria. To verify this efficiency, we compare events that pass a well-modeled subset of muon-object triggers to those that pass a complimentary trigger from the inclusive set of triggers. The muon-object triggers are modeled by studying $Z \rightarrow \mu\mu$ events in data, and good agreement is observed between data and MC when using this subset of triggers. The efficiency of the complimentary set of triggers is determined in data and modeled as a function of the scalar sum of jet p_T (H_T). This model provides an additive correction to the efficiency of the muon-object triggers in our MC, and good agreement between data and MC is observed for the combination of all triggers after the correction is applied.

Simulation of background and signal processes relies on the CTEQ6L1 [15] leading-order parton distribution functions for all MC event generators. The PYTHIA [16] MC generator is used for simulating the production of dibosons with inclusive decays (WW , WZ and WZ), $WH \rightarrow \ell\nu b\bar{b}$ and $ZH \rightarrow \ell\ell b\bar{b}$ ($\ell = e, \mu, \text{ or } \tau$). $W(Z)$ +jets events are generated with ALPGEN [17] interfaced to PYTHIA for parton showering and hadronization. ALPGEN samples are produced using the MLM parton-jet matching prescription [17]. $W(Z)$ +jets samples contain $W(Z)jj$ and $W(Z)cj$ processes, while $W(Z)b\bar{b}$ and $W(Z)c\bar{c}$ are generated separately. Single top-quark events are generated using COMPHEP [18] and use PYTHIA for parton evolution and hadronization. All generated events are processed through a full D0 detector simulation (based on GEANT [19]), using the same reconstruction software as used for D0 data. Simulated events are reweighted for differences in trigger efficiencies of MC simulations relative to data, which depend on the analysis channel, data epoch, and event kinematics.

The simulated background processes are normalized to the SM predictions for their cross sections, except for W +jets

events, which are normalized to data before applying b -tagging, where the contamination from signal is expected to be negligible. The relative data/MC normalization factor is found to be 1.0 ± 0.1 from comparisons of data with next-to-leading-order (NLO) predictions for W +jets based on the MCFM program [20], where the normalization factor for data is obtained after subtracting all other expected background processes. For the W +heavy-flavor jet events, the phenomenological ratio of leading-order to NLO corrections for $Wb\bar{b}$ and W +light jets obtained from MCFM is consistent with experiment, so that we do not apply additional corrections, and the corresponding factors are also used for the Z +heavy-flavor jet processes.

This analysis is based on the selection of events with only one electron with $p_T > 15$ GeV and $|\eta| < 1.1$ or $1.5 < |\eta| < 2.5$, or only a single muon with $p_T > 15$ GeV and $|\eta| < 1.6$. Events are also required to have an $\cancel{E}_T > 20$ GeV, either two or three jets with $p_T > 20$ GeV (after calibration of the jet energy [21]) and $|\eta| < 2.5$, and that the scalar sum of the p_T of the jets (H_T) exceeds 60 GeV (80 GeV for the 3-jets sample). \cancel{E}_T is calculated from the individual calorimeter cells, except for unclustered energy in cells of the coarse-hadronic layers (the outermost readout layers of the calorimeter), and is corrected for the presence of any muons. All energy corrections to electrons or to jets are propagated into \cancel{E}_T . To suppress multijet background, events with $M_W^T < 40 - 0.5 \cancel{E}_T$ are removed, where M_W^T is the transverse mass of the W candidate. Events with additional charged leptons, isolated from jets, that pass a flavor-dependent p_T threshold ($e p_T > 20$ GeV, $\mu p_T > 15$ GeV and $\tau p_T > 10$ or 15 GeV, depending on τ decay channel) are rejected to decrease dilepton background from Z and $t\bar{t}$ events. Only events with a primary vertex (with at least three tracks) located within ± 40 cm of the nominal longitudinal interaction point, measured along the beam axis, are selected for further analysis.

Leptons candidates are identified in two steps: (i) Each candidate must pass “loose” identification criteria, which for electrons requires 95% of the energy in a shower to be deposited in the EM section of the calorimeter, a calorimeter isolation fraction (ratio of EM energy in a $\mathcal{R} < 0.2$ cone to total other calorimeter energy in a $\mathcal{R} < 0.4$ cone) less than 0.10, specific requirements on the spatial distribution of EM showers, a reconstructed track matched to the EM shower, and specific isolation criteria for that matched track. For the loose muon, we require activity in each layer of the muon system, the timing of scintillator hits to coincide with beam crossings (to veto cosmic-rays), a match of the outer muon with a track in the central tracker, and isolation from jets to reject muons from semileptonic decay of hadrons ($\Delta\mathcal{R} > 0.5$). (ii) The loose leptons then undergo a final “tight” selection: tight electrons have to satisfy more restrictive calorimeter isolation fraction and EM energy proportion criteria (< 0.07 and $> 97\%$, respectively), and satisfy a likelihood test developed on $Z \rightarrow ee$ data based on eight quantities characterizing the EM nature of the particles [22]. Tight muons must satisfy stricter isolation criteria on energy in the calorimeter and momenta of tracks near the trajectory of the muon candidate. Inefficiencies introduced by lepton-identification and isolation criteria are determined from $Z \rightarrow \ell\ell$ data. The final selections rely only on tight leptons, with loose leptons used to determine instrumental effects and multijet background.

Instrumental backgrounds and those from semi-leptonic decays of hadrons, referred to jointly as the multijet background, are estimated from data. The instrumental background is important for the electron channel, where a jet with high EM fraction can pass electron-identification criteria, or a photon can be misidentified as an electron. In the muon channel, the multijet background is less important, and arises mainly from the semi-leptonic decay of heavy quarks, where the muon is misidentified as being isolated.

To estimate the number of events containing a jet passing tight lepton selection, we determine the probability, $f_{T|L}$, for a loose-lepton candidate originating from a jet to also pass tight identification. This is done in events that pass preselection requirements, i.e., containing one loose lepton and two jets, but with small \cancel{E}_T (5 – 15 GeV) and without applying a selection on M_W^T . The total non-multijet background is estimated from MC and subtracted from the data before estimating the contribution from multijet events. A probability $f_{T|L}$ is defined by the ratio of the estimated multijet contribution including only tight leptons to that containing loose leptons (which also includes tight leptons). For electrons, $f_{T|L}$ is determined as a function of electron p_T in three regions of $|\eta|$ and four in $\Delta\phi(\cancel{E}_T, e)$, while for muons it taken as a function of $|\eta|$ for two regions of $\Delta\phi(\cancel{E}_T, \mu)$. The efficiency for a loose lepton to pass the tight identification ($\varepsilon_{T|L}$) is measured in $Z \rightarrow \ell\ell$ events in data, and is modeled as a function of p_T for both electrons and muons. A modified version of the “matrix” method [22] is used to determine the multijet background directly from data, where each event is assigned a weight that contributes to the multijet estimation based on $f_{T|L}$ and $\varepsilon_{T|L}$ as a function of event kinematics. Since $f_{T|L}$ depends on \cancel{E}_T , the scale of this estimate of the multijet background must be adjusted when comparing to data with $\cancel{E}_T > 20$. Before applying b -tagging, we perform a fit to the M_W^T distribution to set the scale of the pure multijet and W +jets backgrounds simultaneously.

Jets are reconstructed using a midpoint cone algorithm [24] with a radius of $\Delta\mathcal{R}_y = \sqrt{(\Delta y)^2 + (\Delta\phi)^2} = 0.5$, where y is the jet rapidity. Identification requirements ensure that the distribution in jet energy for all layers of the calorimeter is reasonable and that jets are not caused by noise or spurious depositions of energy. The difference in efficiency for jet identification and jet resolution between data and simulation is taken into account in the overall MC correction for jet reconstruction efficiency. Comparison of ALPGEN with other generators and with data show some discrepancies in distributions of jet pseudorapidity and dijet angular separations [25]. The data are therefore used to

TABLE I: Summary of event yields for the $\ell + b$ -tagged jet(s) + \cancel{E}_T final state. Events in data are compared with the expected number of ST and DT events in the $W+2$ - and $W+3$ -jets samples, in simulated samples of diboson (labelled “ WZ ” in the table), $W/Z+b\bar{b}$ or $c\bar{c}$ (“ $Wb\bar{b}$ ”), W/Z +light-quark jets (“ W +jets”), top quark (“ $t\bar{t}$ ” and “Single t ”) production, and data-derived multijet background (“MJ”). The WH expectation is given for $m_H = 115$ GeV.

	W+2 jets 1 b -tag	W+2 jets 2 b -tags	W+3 jets 1 b -tag	W+3 jets 2 b -tags
WZ	152.6 ± 7.6	22.5 ± 1.2	33.9 ± 1.6	2.6 ± 1.0
$Wb\bar{b}$	1601 ± 129	346 ± 33	358 ± 28	47.8 ± 4.2
W +jets	1290 ± 66	57.5 ± 3.3	210 ± 11	12.1 ± 1.1
$t\bar{t}$	417 ± 35	177 ± 15	633 ± 51	176 ± 14
Single t	203 ± 15	58.3 ± 4.4	53.6 ± 3.9	13.0 ± 1.0
MJ	663 ± 39	56.5 ± 3.7	186 ± 11	12.7 ± 0.8
Total Bkg.	4326 ± 155	718 ± 37	1474 ± 60	264 ± 15
WH	9.7 ± 0.6	6.5 ± 0.4	2.1 ± 0.1	0.8 ± 0.1
Data	4316	709	1463	301

correct the ALPGEN W +jets and Z +jets MC events by reweighting the simulated η of the leading and second-leading jet and the $\Delta\mathcal{R}$ between the two leading jets in the W/Z +jets samples through the use of polynomial functions that bring into agreement the total simulated background and the high statistics pre- b -tagged data. After this step, the jet distributions in simulations are in agreement with the data over the complete range of kinematics.

Efficient identification of b -jets is central to the search for WH production. The D0 neural-network (NN) b -tagging algorithm [23] for identifying heavy-flavored jets is based on a combination of seven variables sensitive to the presence of tracks or secondary vertices displaced significantly from the primary vertex. All tagging efficiencies are determined from data and from simulated events. We choose a “loose” NN operating point that corresponds to a misidentification rate of $\approx 1.5\%$ for “light” partons jets (u, d, s, g) of jet $p_T \approx 50$ GeV that are mistakenly tagged as heavy-flavored jets. If two jets are tagged, the event is selected as double- b -tagged (DT). Events that are not DT are considered for placement in the orthogonal single- b -tag (ST) sample, which requires that a single jet satisfies a “tight” NN operating point corresponding to a mistag rate of about 0.5%. This definition of two orthogonal samples, DT and ST, improves sensitivity to a potential signal beyond choosing a single b -tagging category. The efficiencies for identifying a jet containing a b hadron for the loose and tight NN operating points are $59 \pm 1\%$ and $48 \pm 1\%$, respectively, for a jet p_T of ≈ 50 GeV. The efficiency is determined for taggable jets, i.e., jets with at least 2 tracks of good quality with at least one hit in the SMT. Simulated events are corrected to have the same fraction of jets satisfying the taggability and b -tagging requirements as found in preselected data.

After applying these selection criteria, the expected event yields for specific backgrounds and for a Higgs boson with $m_H = 115$ GeV are compared to the observed number of events in Table I. Distributions of the dijet invariant mass, using the two jets of highest p_T , in $W+2$ -jets and $W+3$ -jets events are shown for the ST and DT samples in Fig. 1(a–d). The data are well described by the sum of the simulated SM processes and multijet background. The contributions expected from a Higgs boson with $m_H = 115$ GeV are also shown.

A RF discriminator [10, 11] uses the following twenty kinematic variables as inputs: $p_{T(\text{leading jet})}$, $p_{T(\text{second leading jet})}$, second leading jet energy, $\Delta\mathcal{R}(\text{leading two jets})$, $\Delta\phi(\text{leading two jets})$, $\Delta\phi(\text{leading jet}, \ell)$, $p_{T(\text{dijet system})}$, dijet invariant mass and $p_{T(\ell-\cancel{E}_T \text{ system})}$, \cancel{E}_T , aplanarity (total p_T -component transverse to the dijet- $(\ell+\cancel{E}_T)$ plane), invariant mass of the $\nu+\ell$ +dijet system ($\sqrt{\hat{s}}$), $\Delta\mathcal{R}(\text{dijet system}, \ell+\nu \text{ system})$, lepton- \cancel{E}_T invariant mass, H_T and H_Z (scalar sum of the transverse and longitudinal momenta of all jets in the event, respectively), and $\cos\theta^*$ and $\cos\chi$, cosines of correlation angles described in [27]. There are separate forests for each Higgs mass considered, with m_H varying between 100–150 GeV in 5 GeV steps, for each of the 12 independent channels. All channels are considered simultaneously when performing our search and final limit setting.

The dijet mass is sensitive to WH production, and has previously been used alone to set limits on $\sigma(p\bar{p} \rightarrow WH)$ [5]. The gain in sensitivity using this random forest approach compared to using only the dijet mass as a discriminant (measured in terms of the expected limit on the WH cross section) is of the order of 20%, depending on the Higgs mass, and is equivalent to a gain of about 40% in integrated luminosity.

The systematic uncertainties from differences in efficiencies between data and MC and from the propagation of other systematic uncertainties (trigger, energy calibration, resolution), which affect the signal and SM backgrounds (but not multijet background), are summarized below. We assume that some of these systematics affect only the normalization of the signal or backgrounds, while others also affect the differential distribution of the dijet invariant mass and RF discriminant. The uncertainty on the measured luminosity is 6.1% [26]. An uncertainty of 3–5% on trigger efficiency is derived from data, as is a 5–6% uncertainty on lepton identification and reconstruction efficiency,

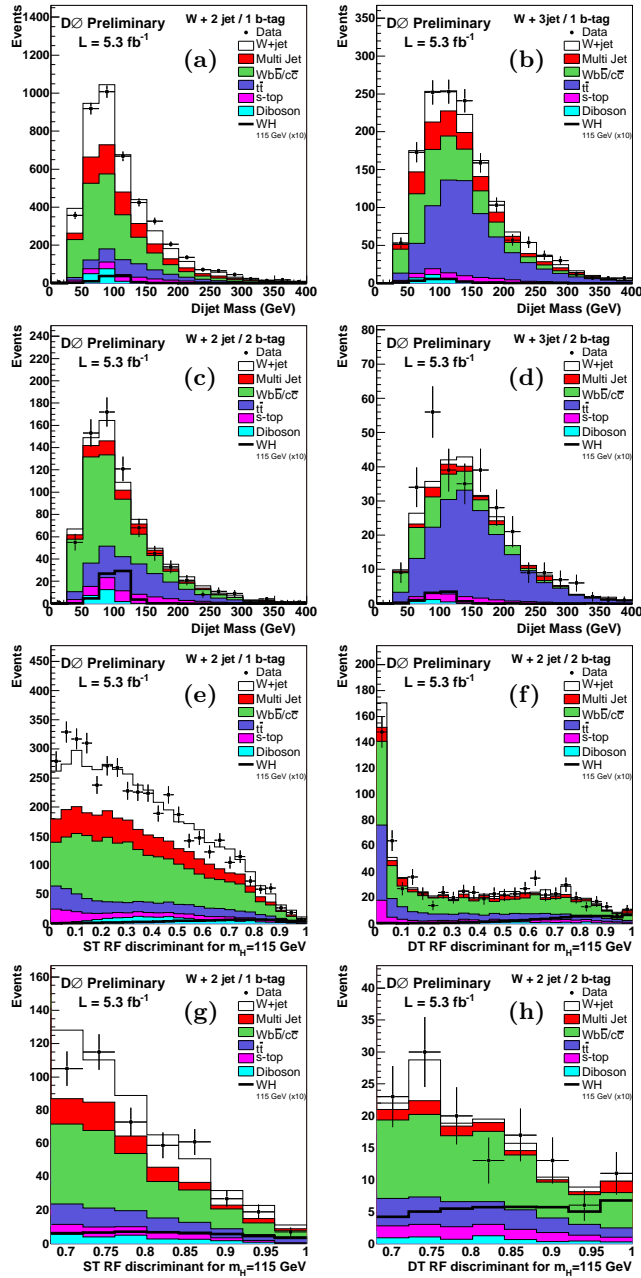


FIG. 1: Dijet mass distributions for the $W+2$ -jets, $W+3$ -jets ST events (a,c) and DT (b,d) events. The data are compared to the background prediction. The distributions in the random forest discriminant for $W+2$ -jet ST and DT events are shown in (e,f), respectively. These distributions are shown for the high RF-output region only in (g,h). The expectation from $10 \times \sigma(p\bar{p} \rightarrow WH)$ for $m_H = 115$ GeV is overlaid.

3% for jet taggability, 2.5–3% for b -tagging efficiency per heavy quark-jet and 10% for mistagging light-quark jets as b -jets. All this translates into an uncertainty on the total background in the exclusive ST sample of 6% (negligible for DT), 5% uncertainty on acceptance for jet identification, jet energy calibration and uncertainty on resolution. The systematic uncertainty on the reweighting of ALPGEN MC samples are of the order of 2%. The “MLM” reweighting applied to W/Z +light-jets and the systematics associated with the choice of renormalization, factorization and α_S scales in ALPGEN, are also of the order of 2% [17].

The systematics on jet-energy calibration, jet resolution and reweighting of MC samples generated with ALPGEN affect the differential distribution of the final discriminant. Overall, the systematic uncertainty on acceptance varies between 16–30%, depending on the process and channel ($\approx 15\%$ for WH in the DT channel). The uncertainty on the

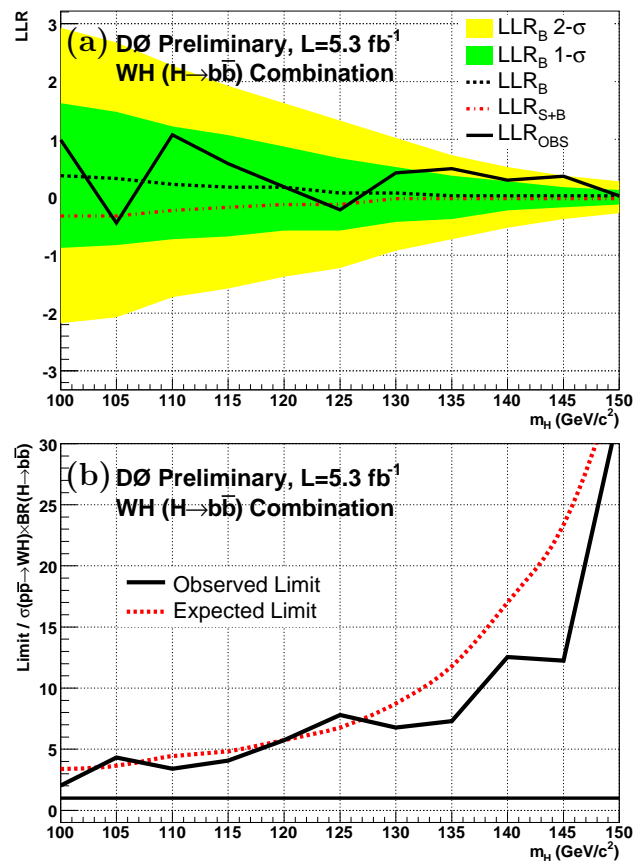


FIG. 2: (a) Log-likelihood ratio for the background-only model (LLR_B , with 1σ and 2σ uncertainty bands), signal+background model (LLR_{S+B}) and observation in data (LLR_{OBS}) vs. m_H . (b) 95% C.L. cross section upper limit (and corresponding expected limit) on $\sigma(p\bar{p} \rightarrow WH) \times \mathcal{B}(H \rightarrow b\bar{b})$ relative to the SM expectation vs. m_H .

TABLE II: Observed and expected 95% C.L. upper limits on the ratio of $\sigma(p\bar{p} \rightarrow WH) \times \mathcal{B}(H \rightarrow b\bar{b})$ to its SM expectation for each m_H value considered.

m_H [GeV]	100	105	110	115	120	125	130	135	140	145	150
Exp. ratio	3.4	3.6	4.4	4.8	5.7	6.8	8.7	11.8	17.0	23.4	36.2
Obs. ratio	2.0	4.3	3.4	4.1	5.7	7.8	6.8	7.3	12.6	12.2	32.7

cross sections for background processes is 10% (12%) for $t\bar{t}$ (single top-quark) production [28, 29], and 6% for diboson production. The uncertainty on W +heavy-flavor production is 20%.

As no excess relative to expectation from SM background is observed, we set upper limits on $\sigma(WH)$ using RF discriminants for the different channels. All bins of the RF distribution are examined to assure good Monte Carlo statistics. Those bins that do not have good statistics are combined with adjacent bins until a smooth distribution that does not sacrifice sensitivity is assured. As described above, each channel is analyzed independently and the limits are then combined. We calculate all limits at 95% C.L. using the modified Frequentist CL_s approach with a Poisson log-likelihood ratio as the test statistic [30, 31]. The likelihood ratio is parameterized by treating systematics as nuisance parameters within their uncertainties, and best fit values of these parameters are determined at each m_H value by maximizing the likelihood. All correlations are maintained among channels and between signal and background.

The upper limit at 95% C.L. on the cross section for $\sigma(p\bar{p} \rightarrow WH) \times \mathcal{B}(H \rightarrow b\bar{b})$ is a factor of 4.1 larger than the SM expectation, for $m_H = 115$ GeV. The corresponding upper limit expected from the SM cross section and our sensitivity is 4.8. The same study is performed for ten other m_H values 100 and 150 GeV. The corresponding observed and expected 95% C.L. limits relative to SM expectation are given in Table II and in Fig. 2.

In conclusion, the $\ell + \cancel{E}_T + 2$ - or 3-jets final states have been analyzed in a search for WH production in 5.3 fb^{-1} of data. The production of single and double b -tagged jets in these events is in agreement with the expected background. We have set upper limits on $\sigma(p\bar{p} \rightarrow WH) \times \mathcal{B}(H \rightarrow b\bar{b})$ relative to its SM expectation for Higgs masses between 100 and 150 GeV, as summarized in Table II and shown in Fig. 2b. For $m_H = 115 \text{ GeV}$, the observed (expected) 95% C.L. limit/SM is 4.8 (4.1).

We thank the staffs at Fermilab and collaborating institutions, and acknowledge support from the DOE and NSF (USA); CEA and CNRS/IN2P3 (France); FASI, Rosatom and RFBR (Russia); CNPq, FAPERJ, FAPESP and FUNDUNESP (Brazil); DAE and DST (India); Colciencias (Colombia); CONACyT (Mexico); KRF and KOSEF (Korea); CONICET and UBACyT (Argentina); FOM (The Netherlands); STFC and the Royal Society (United Kingdom); MSMT and GACR (Czech Republic); CRC Program and NSERC (Canada); BMBF and DFG (Germany); SFI (Ireland); The Swedish Research Council (Sweden); and CAS and CNSF (China).

-
- [1] ALEPH, DELPHI, L3, and OPAL Collaborations, The LEP Working Group for Higgs Boson Searches, *Phys. Lett. B* **565**, 61 (2003).
- [2] LEP Electroweak Working Group,
<http://lepewwg.web.cern.ch/LEPEWWG/>
- [3] . CDF and D0 Collaboration, T. Aaltonen *et al.*, *Phys. Rev. Lett.* 104, 061802 (2010).
- [4] D0 Collaboration, V.M. Abazov *et al.*, *Phys. Rev. Lett.* 94, 091802 (2005).
- [5] D0 Collaboration, V.M. Abazov *et al.*, *Phys. Lett. B* 663, 26 (2008).
- [6] D0 Collaboration, V.M. Abazov *et al.*, *Phys. Rev. Lett.* 102, 051803 (2009).
- [7] CDF Collaboration, D. Acosta *et al.*, *Phys. Rev. Lett.* 94, 091802 (2005).
- [8] CDF Collaboration, T. Aaltonen *et al.*, *Phys. Rev. Lett.* 100, 041801 (2008).
- [9] CDF Collaboration, T. Aaltonen *et al.*, *Phys. Rev. Lett.* 103, 101802 (2009).
- [10] L. Breiman, *Machine Learning* **45**, 5 (2001).
- [11] I. Narsky, arXiv:physics/0507143 [physics.data-an] (2005).
- [12] DØ Collaboration, V. Abazov *et al.*, *Nucl. Instrum. Meth., Res. A* 565, 463 (2006).
- [13] Pseudorapidity $\eta = -\ln \left[\tan \frac{\theta}{2} \right]$, where θ is the polar angle as measured from the beam axis; ϕ is the azimuthal angle. The separation between two objects in η, ϕ space is $\Delta\mathcal{R} = \sqrt{(\Delta\eta)^2 + (\Delta\phi)^2}$.
- [14] S. Abachi, *et al.*, *Nucl. Instrum. Methods Phys. Res. A* 338, 185 (1994).
- [15] H. L. Lai *et al.*, *Phys.Rev. D*55 (1997) 1280, <http://hep.pa.msu.edu/people/wkt/cteq6/cteq6pdf.html>
J. Pumplin *et al.*, *JHEP07(2002)012*, arXiv:hep-ph/0201195v3.
- [16] T. Sjostrand, P. Eden, C. Friberg, L. Lonnblad, G. Miu, S. Mrenna and E. Norrbin, *Comput. Phys. Commun.* 135, (2001) 238, versions 6.319, 6.323 and 6.409.
- [17] M. Mangano *et al.*, ALPGEN, hep-ph/0206293, *JHEP07* (2003) 001, version 2.05, <http://mlm.web.cern.ch/mlm/alpgen>
- [18] A. Pukhov *et al.*, COMPHEP, hep-ph/9908288 (1999)
- [19] R. Brun and F. Carminati, CERN Program library Long Writeup, Report W5013 (1993).
- [20] J. Campbell and K. Ellis, MCFM, <http://mcfm.fnal.gov/>
- [21] J. Hegeman, *J. Phys. Conf. Ser.* **160**, 012024 (2009).
- [22] DØ Collaboration, V. Abazov *et al.*, *Phys. Rev. D* 76, 092007 (2007)
- [23] T. Scanlon, FERMILAB-THESIS-2006-43 (2006)
- [24] G. Blazey *et al.*, in *Proceedings of the workshop "QCD and Weak Boson Physics in Run II"* edited by U. Baur, R.K. Ellis, and D. Zeppenfeld, Batavia (2000), p. 47. arXiv:hep-ex/0005012 (2000).
- [25] J. Alwall *et al.*, *Eur. Phys. C* 53, 473 (2008).
- [26] T. Andeen, *et al.*, FERMILAB-TM-2365, April 2007.
- [27] S. Parke and S. Veseli, *Phys. Rev. D* **60**, 093003 (1999).
- [28] N. Kidonakis *et al.*, *Phys. Rev. D* 78, 074005 (2008).
- [29] N. Kidonakis, *Phys. Rev. D* 74, 114012 (2006).
- [30] T. Junk, *Nucl. Instrum. Meth. A*434, p. 435-443, 1999.
- [31] W. Fisher, FERMILAB-TM-2386-E (2007).